Primitive Variable, Strongly Implicit Calculation Procedure for Viscous Flows at All Speeds

K.-H. Chen* and R. H. Pletcher†
Iowa State University, Ames, Iowa 50011

A coupled solution procedure is described for solving the compressible form of the time-dependent, two-dimensional Navier-Stokes equations in body-fitted curvilinear coordinates. This approach employs the strong conservation form of the governing equations but uses primitive variables (u, v, p, T) rather than the more traditional conservative variables (ρ, ρu, ρv, e_t) as unknowns. A coupled modified strongly implicit procedure (CMSIP) is used to efficiently solve the Newton-linearized algebraic equations. It appears that this procedure is effective for Mach numbers ranging from the incompressible limit ($M_\infty \sim 0.01$) to supersonic. Generally, smoothing was not needed to control spatial oscillations in pressure for subsonic flows despite the use of central differences. Dual-time stepping was found to further accelerate convergence for steady flows. Sample calculations, including steady and unsteady low-Mach-number internal and external flows and a steady shock-boundary-layer interaction flow, illustrate the capability of the present solution algorithm.

Introduction

OVER the past two decades, a number of different finite-difference schemes have been proposed to solve the Navier-Stokes equations.[1] Traditionally, they have been classified as methods for either compressible or incompressible flows. Most of the formulations for compressible flows have utilized conservative variables,[2,3] which include density, instead of pressure, as a primary variable, and the equations have generally been solved in a coupled (simultaneous) manner. An exception to this is the recent work of Karki and Patankar[4] and Van Doormaal et al.[5]

Methods for incompressible flows, on the other hand, have employed a wider range of dependent variables, including derived as well as primitive, and the equations have generally been solved in a segregated (one variable at a time) manner. The derived variable approaches usually either involve more unknowns than contained in the original Navier-Stokes equations or become too complicated to easily extend to three-dimensional flow calculations.

Numerical methods developed for compressible flows are not, in general, suitable for efficiently solving low-Mach-number or incompressible flows. The reasons usually offered for this are 1) roundoff error due to using density as a primary variable,[6] 2) truncation errors due to applying approximate factorization in multiple dimensional problems,[7] and 3) a time step (or CFL number) constraint due to near infinite acoustic speed.[1]

To circumvent some of the above problems, pressure can be chosen as a primary variable instead of density because the variation of pressure is generally significant for all flow regimes. This idea has been used[8] in solving low-Mach-number steady flows by a coupled space marching procedure that involves using multiple sweeps to account for the upstream propagation of pressure signals. But this space marching procedure is only effective for flows within a dominant flow direction. Recently, a similar idea, although different in detail, was proposed to alleviate the above problems using a segregated algorithm.[4] Feng and Merkle[9] also employed pressure as a primary variable in a scheme that utilized a preconditioning technique to scale all eigenvalues of the coupled system of equations to the same order of magnitude in order to accelerate convergence for low-Mach-number steady flows.

The approximate factorization procedure was avoided in the present work by using a modified form of Stone's strongly implicit procedure (SIP)[10] to solve the algebraic equations in the plane. The modified form of the SIP algorithm (MSIP) proposed by Schneider and Zedan[11] exhibits faster convergence and less sensitivity to the relaxation-type parameter of the method than the original SIP algorithm. The MSIP algorithm was extended to handle a coupled 4×4 block system in the present work.

There are many applications in which it would be convenient to use the same algorithm for Mach numbers ranging from incompressible to transonic. The search for an algorithm suitable for all speeds goes back at least to the work of Harlow and Amsden.[12] More recent work on the subject includes contributions from Karki and Patankar[4] and Van Doormaal et al.[5] The main contribution of the present work is to point out a solution strategy that could be applied to a number of difference formulations to permit efficient computation over a wider range of Mach numbers. The specific difference stencil used in the present work may not be optimum for all cases (particularly at very high Reynolds number), and can clearly be improved. The form used, however, does serve to illustrate the advantages of the overall approach.

In the present paper, a coupled strongly implicit procedure for solving the two-dimensional unsteady compressible conservation-law form of the Navier-Stokes equations with primitive variables, i.e., u and v velocity components, pressure, and temperature, is described. Incompressible test cases are computed from this formulation simply by setting the Mach number to a very low value. Since all variables, including pressure, are computed simultaneously in the algorithm, there is no need to use a separate pressure Poisson equation, and the continuity equation is automatically satisfied. Some convergence enhancement techniques for steady-state solutions will also be described. Several steady-state results including two low-Mach-number incompressible flows and one supersonic flow will be given. One unsteady subsonic flow is also discussed.

Presented as Paper 90-1521 at the AIAA 21st Fluid Dynamics, Plasma Dynamics, and Lasers Conference, Seattle, WA, June 18–20, 1990; received June 25, 1990; revision received Dec. 18, 1990; accepted for publication Dec. 27, 1990.

*Research Assistant, Department of Mechanical Engineering and Computational Fluid Dynamics Center, 2025 H. M. Black Engineering Building; currently at the University of Toledo/NASA Lewis Research Center, Cleveland, OH. Member AIAA.

†Professor, Department of Mechanical Engineering and Computational Fluid Dynamics Center, 2025 H. M. Black Engineering Building. Member AIAA.

Numerical Approach

Governing Equations

After replacing the density by pressure and temperature using the equation of state ($\rho = p/RT$), the nondimensional form of the unsteady, two-dimensional compressible Navier-Stokes equations can be written in generalized nonorthogonal coordinates[1] as

$$\frac{\partial Q(q)}{\partial \tau} + \frac{\partial E(q)}{\partial \xi} + \frac{\partial F(q)}{\partial \eta} = 0 \tag{1}$$

where

$$q = \begin{pmatrix} u \\ v \\ p \\ T \end{pmatrix}$$

$$Q = \frac{1}{J}\begin{bmatrix} \frac{pu}{T} \\ \frac{pv}{T} \\ \frac{p}{T} \\ (C_p - R)p + \frac{1}{2}\frac{pu^2}{T} + \frac{1}{2}\frac{pv^2}{T} \end{bmatrix}$$

$$E = \frac{1}{J}\begin{bmatrix} \frac{p}{T}uU + Rp\xi_x - (\xi_x\tau_{xx} + \xi_y\tau_{xy}) \\ \frac{p}{T}vU + Rp\xi_y - (\xi_x\tau_{xy} + \xi_y\tau_{yy}) \\ \frac{p}{T}U \\ \left(C_p p + \frac{p}{T}\frac{u^2}{2} + \frac{p}{T}\frac{v^2}{2}\right)U \\ -\xi_x u\tau_{xx} - (\xi_x v + \xi_y u)\tau_{xy} - \xi_y v\tau_{yy} \\ -\frac{RC_p\mu}{PrRe}[(\xi_x^2 + \xi_y^2)T_\xi + (\xi_x\eta_x + \xi_y\eta_y)T_\eta] \end{bmatrix}$$

$$F = \frac{1}{J}\begin{bmatrix} \frac{p}{T}uV + Rp\eta_x - (\eta_x\tau_{xx} + \eta_y\tau_{xy}) \\ \frac{p}{T}uV + Rp\eta_y - (\eta_x\tau_{xy} + \eta_y\tau_{yy}) \\ \frac{p}{T}V \\ \left(C_p p + \frac{p}{T}\frac{u^2}{2} + \frac{p}{T}\frac{v^2}{2}\right)V \\ -\eta_x u\tau_{xx} - (\eta_x v + \eta_y u)\tau_{xy} - \eta_y v\tau_{yy} \\ -\frac{RC_p\mu}{PrRe}[(\xi_x\eta_x + \xi_y\eta_y)T_\xi + (\eta_x^2 + \eta_y^2)T_\eta] \end{bmatrix}$$

$$\tau_{xx} = \frac{2}{3}\frac{R\mu}{Re}[2(\xi_x u_\xi + \eta_x u_\eta) - (\xi_y v_\xi + \eta_y v_\eta)]$$

$$\tau_{yy} = \frac{2}{3}\frac{R\mu}{Re}[2(\xi_y v_\xi + \eta_y v_\eta) - (\xi_x u_\xi + \eta_x u_\eta)]$$

$$\tau_{xy} = \frac{R\mu}{Re}[(\xi_y u_\xi + \eta_y u_\eta) - (\xi_x v_\xi + \eta_x v_\eta)]$$

$$U = \xi_x u + \xi_y v \qquad V = \eta_x u + \eta_y v$$

Laminar flow was assumed and the viscosity for air was determined by the Sutherland formula[1] as follows:

$$\mu = \frac{C_1 T^{3/2}}{(T + C_2)} \tag{2}$$

The above nondimensional variables were defined in the following manner (dimensional quantities are indicated by a tilde):

$$t = \frac{\tilde{t}}{L_{\text{ref}}/u_{\text{ref}}}, \quad x = \frac{\tilde{x}}{L_{\text{ref}}}, \quad y = \frac{\tilde{y}}{L_{\text{ref}}}, \quad u = \frac{\tilde{u}}{u_{\text{ref}}}$$

$$v = \frac{\tilde{v}}{u_{\text{ref}}}, \quad \rho = \frac{\tilde{\rho}}{\rho_{\text{ref}}}, \quad p = \frac{\tilde{p}}{(\rho_{\text{ref}}u_{\text{ref}}^2)}, \quad T = \frac{\tilde{T}}{T_{\text{ref}}}$$

$$\mu = \frac{\tilde{\mu}}{\mu_{\text{ref}}}, \quad C_1 = \tilde{C}_1\frac{T_{\text{ref}}^{1/2}}{\mu_{\text{ref}}}, \quad C_2 = \frac{\tilde{C}_2}{T_{\text{ref}}}$$

$$R = \frac{\tilde{R}}{(u_{\text{ref}}^2/T_{\text{ref}})} = \frac{1}{\gamma M_\infty^2}$$

$$C_p = \frac{\tilde{C}_p}{(u_{\text{ref}}^2/T_{\text{ref}})} = \frac{1}{(\gamma - 1)M_\infty^2}$$

The Reynolds number, Mach number, and Prandtl number were defined as

$$Re = \frac{\rho_{\text{ref}}u_{\text{ref}}L_{\text{ref}}}{\mu_{\text{ref}}}, \quad M_\infty = \frac{u_{\text{ref}}}{\sqrt{\gamma\tilde{R}T_{\text{ref}}}}, \quad Pr = \frac{\tilde{C}_p\tilde{\mu}}{\tilde{k}}$$

Here, L_{ref} is a flowfield characteristic length; x and y are the Cartesian coordinates; u and v are the respective Cartesian velocity components; ρ is the density; p is the static pressure; μ is the dynamic viscosity; T is the static temperature; R is the gas constant; C_p is the constant pressure specific heat; k is the thermal conductivity; γ is the specific heat ratio; and C_1 and C_2 are the Sutherland constants. The subscript "ref" denotes the reference quantities that are the upstream bulk properties for internal flow cases, or the freestream properties for external flow cases.

All sample calculations were performed for dry air at ambient temperature and pressure using the following fluid property constants.

$$\tilde{R} = 287 \text{ m}^2/(\text{s}^2\text{ K}), \qquad \gamma = 1.4$$

$$\tilde{C}_1 = 1.458 \times 10^{-6} \text{ kg/(m s }\sqrt{\text{K}}), \qquad \tilde{C}_2 = 110.4 \text{ K}$$

Discretization of the Equations

The discretization will be described for the form of the equations given by Eq. (1). A first-order forward difference was used for the time terms. Central differences, in general, were used for the spatial derivative terms in the equations. For example, the first-order spatial derivative term of the continuity equation in the ξ direction was differenced by

$$\frac{\partial}{\partial\xi}\left(\frac{pU}{JT}\right)_{i,j}^{n+1} = \frac{1}{2}\left[\left(\frac{pU}{JT}\right)_{i+1,j}^{n+1} - \left(\frac{pU}{JT}\right)_{i+1,j}^{n+1}\right]$$

where, $\Delta\xi = 1$ was assumed. However, the deferred correction formula proposed by Khosla and Rubin[13] was also used for the convective terms in the momentum and energy equations for one of the cases presented in this paper (driven cavity flow). For example,

$$\frac{\partial}{\partial\xi}\left(\frac{puU}{JT}\right)_{i,j}^{n+1,k+1} = \left[\left(\frac{puU}{JT}\right)_{i,j}^{n+1,k+1} - \left(\frac{puU}{JT}\right)_{i-1,j}^{n+1,k+1}\right] + \frac{1}{2}\left[\left(\frac{puU}{JT}\right)_{i+1,j}^{n+1,k} - 2\left(\frac{puU}{JT}\right)_{i,j}^{n+1,k} + \left(\frac{puU}{JT}\right)_{i-1,j}^{n+1,k}\right]$$

for $U > 0$ (3)

$$\frac{\partial}{\partial\xi}\left(\frac{puU}{JT}\right)_{i,j}^{n+1,k+1} = \left[\left(\frac{puU}{JT}\right)_{i+1,j}^{n+1,k+1} - \left(\frac{puU}{JT}\right)_{i,j}^{n+1,k+1}\right] - \frac{1}{2}\left[\left(\frac{puU}{JT}\right)_{i+1,j}^{n+1,k} - 2\left(\frac{puU}{JT}\right)_{i,j}^{n+1,k} + \left(\frac{puU}{JT}\right)_{i-1,j}^{n+1,k}\right] \quad \text{for } U < 0 \quad (4)$$

The upwind-differencing part of the above expression was evaluated implicitly on the left-hand side of the equations and the central-differencing part was evaluated explicitly on the right-hand side of the equations. When the solution converges, the second-order central difference is recovered.

The second-order spatial derivative terms in the ξ direction were differenced as

$$\frac{\partial}{\partial\xi}\left(a\frac{\partial\phi}{\partial\xi}\right)_{i,j}^{n+1} = \left(a\frac{\partial\phi}{\partial\xi}\right)_{i+1/2,j}^{n+1} - \left(a\frac{\partial\phi}{\partial\xi}\right)_{i-1/2,j}^{n+1}$$

where ϕ is the dependent variable, a represents a combination of metric terms and viscosity in the viscous terms in the momentum equations and the coefficient to the conduction terms in the energy equation, $(i + 1/2)$ indicates a location halfway between i and $(i + 1)$, and $(i - 1/2)$ denotes a location halfway between $(i - 1)$ and i. The values of $a_{i+1/2}$ and $a_{i-1/2}$ were determined as

$$a_{i+1/2,j} = \tfrac{1}{2}(a_{i,j} + a_{i+1,j}), \qquad a_{i-1/2,j} = \tfrac{1}{2}(a_{i,j} + a_{i-1,j})$$

and the first-order derivative terms at the half-nodal point were evaluated as

$$\left(\frac{\partial\phi}{\partial\xi}\right)_{i+1/2,j}^{n+1} = \phi_{i+1,j}^{n+1} - \phi_{i,j}^{n+1}$$

$$\left(\frac{\partial\phi}{\partial\xi}\right)_{i-1/2,j}^{n+1} = \phi_{i,j}^{n+1} - \phi_{i-1,j}^{n+1}$$

Similar expressions for the terms in the η direction are evaluated in the same way. The second-order spatial cross derivative terms are expressed as

$$\frac{\partial\phi}{\partial\xi}\left(\frac{\partial\phi}{\partial\eta}\right)_{i,j}^{n+1} = \tfrac{1}{4}(\phi_{i+1,j+1}^{n+1} - \phi_{i+1,j-1}^{n+1} - \phi_{i-1,j+1}^{n+1} + \phi_{i-1,j-1}^{n+1})$$

The above central-difference representations for the spatial derivative terms can also be interpreted as evaluating the flux quantities [E and F in the Eq. (1)] at the face of control volume by simply averaging the flux quantities at two nodal points, e.g., $E_{i+1/2,j} = \frac{1}{2}(E_{i+1,j} + E_{i-1,j})$. All metric terms of the transformation at the interior points were evaluated by second-order central differences satisfying the geometric conservation law.[14]

After differencing, all nonlinear terms were linearized by a Newton method.[1] However, it should be noted that an equivalent formulation can be developed using conventional Jacobian matrices.[15] The representations for two typical nonlinear terms, such as the time term in the continuity equation and one of the convective terms in the momentum equations, are illustrated as

$$\left(\frac{p}{T}\right)^{n+1,k+1} \simeq \left(\frac{1}{T}\right)^{n+1,k} p^{n+1,k+1} - \left(\frac{p}{T^2}\right)^{n+1,k} T^{n+1,k+1} + \left(\frac{p}{T}\right)^{n+1,k} \quad (5)$$

$$\left(\frac{puU}{JT}\right)^{n+1,k+1} \simeq \left(\frac{pU}{JT} + \frac{pu}{T}y_\eta\right)^{n+1,k} u^{n+1,k+1} - \left(\frac{pu}{T}x_\eta\right)^{n+1,k} v^{n+1,k+1} + \left(\frac{uU}{JT}\right)^{n+1,k} p^{n+1,k+1} - \left(\frac{puU}{JT^2}\right)^{n+1,k} T^{n+1,k+1} - \left(\frac{puU}{JT}\right)^{n+1,k} \quad (6)$$

where k is the iteration index and n indicates the time level.

For time-accurate calculations, the linearization error can be effectively removed by iterating at each time level. For steady-state calculations, iterations were not required at each time step since the time marching scheme is itself a relaxation procedure. All terms were treated in an implicit way (at level $n + 1$, $k + 1$) except the viscous dissipation terms (in the energy equation) that were evaluated at the level $(n + 1, k)$. After linearization, the four variables, u, v, p, and T, appear in all of the equations and the resulting equations takes the following form:

$$A_{i,j}^6\boldsymbol{q}_{i-1,j-1} + A_{i,j}^5\boldsymbol{q}_{i+1,j-1} + A_{i,j}^4\boldsymbol{q}_{i+1,j-1} + A_{i,j}^7\boldsymbol{q}_{i-1,j} + A_{i,j}^9\boldsymbol{q}_{i,j} + A_{i,j}^3\boldsymbol{q}_{i+1,j} + A_{i,j}^8\boldsymbol{q}_{i-1,j+1} + A_{i,j}^1\boldsymbol{q}_{i,j+1} + A_{i,j}^2\boldsymbol{q}_{i+1,j+1} = \boldsymbol{b}_{i,j} \quad (7)$$

and can be expressed in a matrix form as

$$[A]\boldsymbol{q} = \boldsymbol{b} \quad (8)$$

where

$$[A] = \begin{bmatrix} A_{1,1}^9 & A_{1,1}^3 & & A_{1,1}^1 & A_{1,1}^2 & & & & \\ A_{i,j}^6 & A_{i,j}^5 & A_{i,j}^4 & A_{i,j}^7 & A_{i,j}^9 & A_{i,j}^3 & & A_{i,j}^8 & A_{i,j}^1 & A_{i,j}^2 \\ & & & & A_{im,jm}^6 & A_{im,jm}^5 & & A_{im,jm}^7 & A_{im,jm}^9 \end{bmatrix}$$

is the coefficient matrix with a 4×4 block in each element and

$$\boldsymbol{q} = [(u, v, p, T)_{1,1}^T, \ldots, (u, v, p, T)_{i,j}^T, \ldots, (u, v, p, T)_{im,jm}^T]^T$$

$$\boldsymbol{b} = [(b_u, b_v, b_p, b_T)_{1,1}^T, \ldots, (b_u, b_v, b_p, b_T)_{i,j}^T, \ldots, (b_u, b_v, b_p, b_T)_{im,jm}^T]^T$$

are the unknown vector and the right-hand side vector, respectively. Figure 1 shows the computational molecule for A^1, A^2, A^3, . . . and A^9.

Boundary Conditions

All boundary conditions were treated implicitly. In general, except for noslip boundaries, the governing equations were written on boundary points. This procedure usually needs field variables at the points outside the domain. The way the unknowns at these extra points are determined varies with the boundary and flow types. The various boundary conditions are discussed as follows:

Inflow Boundary

For subsonic flows, u, v, and T were specified. Pressure was extrapolated from interior points. For supersonic flows, all variables must be specified.

Outflow Boundary

For subsonic flows, pressure was specified at this boundary and extrapolation was used to obtain other variables. For supersonic flows, all variables were extrapolated from interior points.

Far-Field Boundary

For subsonic flows, freestream velocity, pressure, and temperature were specified and the v component of velocity was

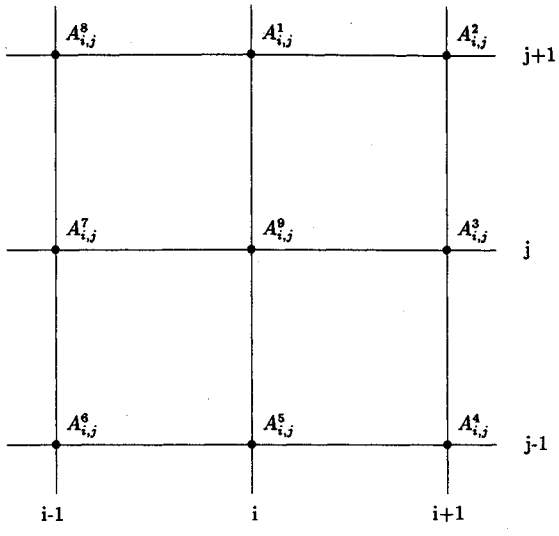

Fig. 1 Computational molecule for $A^1_{i,j}$, $A^2_{i,j}$, . . . , $A^9_{i,j}$.

obtained by extrapolation from interior points. For supersonic flows reported in this paper, all variables were specified.

Symmetry Boundary

The governing equations were written at this boundary as described above. All variables at the points outside the domain were obtained by the symmetry condition for u, p, and T and the antisymmetry condition for v.

Wall Boundary

Instead of writing the governing equations at this boundary, noslip conditions were used for velocity components. Either isothermal or a heat flux condition was used for the boundary condition for T. For pressure, the favored treatment is to write the normal momentum equation at this boundary and apply the noslip conditions to simplify it. The resulting equation will relate the normal derivative of pressure to velocity derivative terms. The treatment will become more complicated for irregular or curvilinear boundaries but it may enhance the coupling between the pressure and velocity fields and avoid spurious pressure solutions. This idea will be discussed further in the results section.

For internal steady-flow calculations, the treatment for the pressure boundary condition at the inflow and outflow deserves special attention. For a compressible formulation used in this study, the pressure level calculated at the inflow boundary must be adjusted (due to density variation) as the calculation proceeds if the specified Reynolds number is to be maintained. The same adjustment must be applied to the pressure everywhere, including the outflow pressure. This pressure adjustment procedure maintains a constant and predetermined mass flow rate. Without this adjustment, the Reynolds number of the final converged solution may drift from the desired value. This drift was found to be more severe for low-Reynolds-number flows.

CMSIP Solution Procedure

The above algebraic equations with the specified boundary conditions, which has a 4 × 4 block in each element, were solved by the CMSIP procedure. This procedure introduces an auxiliary matrix $[P]$ to both sides of the above matrix equation [Eq. (8)] as

$$[A + P]\boldsymbol{q}^{n+1,k+1} = [P]\boldsymbol{q}^{n+1,k} + \boldsymbol{b} \tag{9}$$

where $[A + P]$ can be conveniently decomposed into lower- and upper-block triangular matrices, each of which has only five nonzero diagonals. The following procedure was used to obtain the unknown vector $\boldsymbol{q}$. Letting $\boldsymbol{\delta}^{n+1,k+1} = \boldsymbol{q}^{n+1,k+1} - \boldsymbol{q}^{n+1,k}$ and a residual vector $\boldsymbol{R}^{n+1,k} = \boldsymbol{b} - [A]\boldsymbol{q}^{n+1,k}$, Eq. (9) becomes

$$[A + P]\boldsymbol{\delta}^{n+1,k+1} = \boldsymbol{R}^{n+1,k} \tag{10}$$

Replacing $[A + P]$ by the $[L][U]$ product gives

$$[L][U]\boldsymbol{\delta}^{n+1,k+1} = \boldsymbol{R}^{n+1,k} \tag{11}$$

Defining a provisional vector $\boldsymbol{W}$ by $\boldsymbol{W}^{n+1,k+1} = [U]\boldsymbol{\delta}^{n+1,k+1}$, the solution procedure can be written in two step:

Step 1:

$$[L]\boldsymbol{W}^{n+1,k+1} = \boldsymbol{R}^{n+1,k} \tag{12}$$

Step 2:

$$[U]\boldsymbol{\delta}^{n+1,k+1} = \boldsymbol{W}^{n+1,k+1} \tag{13}$$

The detailed formulation of this procedure can be found in Andersen et al.,[1] Stone's original paper,[10] and Schneider and Zedan[11] for scalar equations. The coupled formula, which is a straightforward extension from its scalar counterpart, can be obtained from Chen[15] or Zedan and Schneider.[16] This procedure treats the unknowns for the entire domain in a strongly implicit manner that enhances the robustness of the solution algorithm. It should be noted that the present work may be one of the first attempts to solve *compressible* Navier-Stokes equations by the CMSIP scheme. Application of the CMSIP scheme to hyperbolic equations has been studied by Walters et al.[17], where a stability analysis showed that the SIP scheme was unconditionally stable for the three-dimensional wave equation.

Smoothing

When a nonstaggered (collocated) grid arrangement is used with central differences, a spatial oscillation in pressure due to pressure-velocity decoupling has frequently been reported in the literature[18] for low-Mach-number and incompressible flows. This type of high-frequency oscillation is also found near a shock wave in supersonic flows. In most cases, for low-Mach-number flow calculations, it appears that this pressure oscillation can be removed by proper treatment of the boundary conditions and the form of governing equations used, although the generality of this finding is still being studied. If the pressure decoupling occurs, the following explicit smoothing procedure (or "filter"[19]) is suggested

$$\phi^{\text{new}} = \phi^{\text{old}} + \omega\left(\frac{\partial^2\phi^{\text{old}}}{\partial\xi^2} + \frac{\partial^2\phi^{\text{old}}}{\partial\eta^2}\right) \tag{14}$$

where ϕ is the variable to be smoothed.

Smoothing was generally not needed in the subsonic flow calculations. The exception was for the cylinder cases where smoothing was required for the pressure. For those cases, the pressure boundary conditions were obtained by setting the pressure derivative normal to the body equal to zero rather than the more usual procedure of evaluating the pressure derivative from the momentum equations. A value of ω between 0.05 and 0.2 was found to be satisfactory. For the supersonic case, all dependent variables were smoothed using $\omega = 0.005$. The widely used implicit smoothing method[1] was also tried and it was found that the present explicit smoothing was less sensitive to the smoothing parameter ω.

Convergence Criterion

The convergence criterion was based on the norm of all variables in a coupled sense. This criterion is as follows:

$$\left(\frac{\sum_{i,j=1}^{im,jm} \sum_{n=1}^{n=4} \left| \frac{q_n^{k+1} - q_n^k}{q_{n,\text{rms}}^{k+1}} \right|^2}{4 \times im \times jm} \right)^{0.5} \leq \varepsilon \qquad (15)$$

where k is the iteration level, n the variable index, im the number of grid points in the x direction, jm the number of grid points in the y direction, q_n a component of the unknown vector $\boldsymbol{q}$, and $q_{n,\text{rms}}$ the root-mean-square value of q_n. The criterion ε was generally set equal to 1.0×10^{-4}.

Convergence Acceleration Technique

As with most central-difference schemes, the time term serves to enhance the diagonal dominance, especially if the continuity equation is solved coupled with the system. When central differences are applied to the spatial derivative terms in the continuity equation, the time term must be retained to avoid a singularity in the matrix system. Unlike the momentum and energy equations that possess nonzero diagonal terms from the diffusion and conduction terms, the time term in the continuity equation bears all of the burden of providing the diagonal dominance in this equation. Although the present method solves equations in a coupled manner, and the resulting coefficient matrix is in block form, the diagonal dominance requirement for a single equation can still provide a good guidelines to assure convergence of the coupled equations. Golub and Van Loan[20] provide the definition of the diagonal dominance for a block system, but it was found impractical to use in the present work.

Consistent with the above observations, the present authors found that if the steady-state solution is the only concern, dual time can be used to accelerate the convergence rate for low-Mach-number flow calculations when an isothermal condition is assumed. This dual-time technique applies a much smaller time step for the continuity equation than for momentum equations. For this current formulation, the time step for the continuity equation was about the order of M_∞^2 for low-Mach-number flows. This dual-time procedure is equivalent to using different relaxation factors for different equations. This technique assures that the rapidly propagating pressure signal in low-Mach-number flows is resolved by the smaller time step used in the continuity equation, which can be thought as an equation for pressure.

The local time step[15] was also used in the momentum and energy equations to further accelerate the convergence for steady state calculations.

Sample Results

Sample results are presented for four subsonic cases and one supersonic case. The four subsonic cases include two steady-state internal flows, one steady-state external flow, and one unsteady external flow. The results for these five test cases are briefly described in the next several sections.

Subsonic Steady-State Flows

Developing Flow in a Channel

Because of the symmetrical nature of this problem, only the upper half-channel was calculated. Four cases with Reynolds numbers of 0.5, 10, 75, and 7500 and a Mach number of 0.05 was studied. The Reynolds number is based on the inlet velocity, bulk density, and half-width of the channel. Grids of 21 × 11, 21 × 11, 31 × 11, and 41 × 11 points and nondimensional channel lengths of 2, 4, 30, and 3000 were used for Reynolds numbers of 0.5, 10, 75, and 7500, respectively. The grid points were clustered near the inlet and the upper wall. The centerline velocity distribution along the flow-development region is shown in Fig. 2. The agreement between the present results and those by TenPas and Pletcher,[8] Morihara and Cheng,[21] McDonald et al.,[22] and Bodoia and Osterle[23] is good. The convergence history of these four cases is shown in Fig. 3. It should be noted that for steady-state calculations, iterations were not used at each time step so that the number of iterations shown in the figure is equal to the number of time steps. Heat transfer at $Re = 500$ and $Pr = 0.72$ was also studied for this case. The results have been reported in Chen and Pletcher[24] and will not be presented here.

Driven Cavity Flow

The two-dimensional driven cavity problem was studied very extensively and served as a benchmark test case for the incompressible Navier-Stokes calculations. Results were obtained for Reynolds numbers of 100, 1000, and 3200, respectively, under an isothermal condition and a Mach number of 0.05. Figure 4 shows the u velocity component along the vertical centerline, and Fig. 5 shows the v velocity component along the horizontal centerline for these three Reynolds numbers. The agreement with the results by Ghia et al.[25] and Goodrich and Soh[26] is excellent for $Re = 100$ and 1000 and is good for $Re = 3200$. The effects of grid refinement are also shown. Figure 6 compares the pressure distribution along the stationary wall obtained by the present method with those obtained by Ghia et al.[27] The abscissa in Fig. 6 represents distance along the parameter of the cavity, measured as indicated in the insert.

The streamline pattern, pressure contours, the velocity vectors for $Re = 3200$ are shown in Fig. 7. For the grid points used (indicated in the figures), the convergence rate for Re

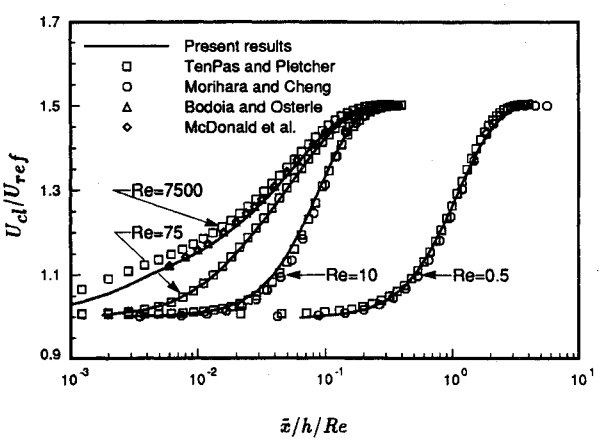

Fig. 2 Predicted centerline velocity distribution for developing flow in a two-dimensional channel inlet.

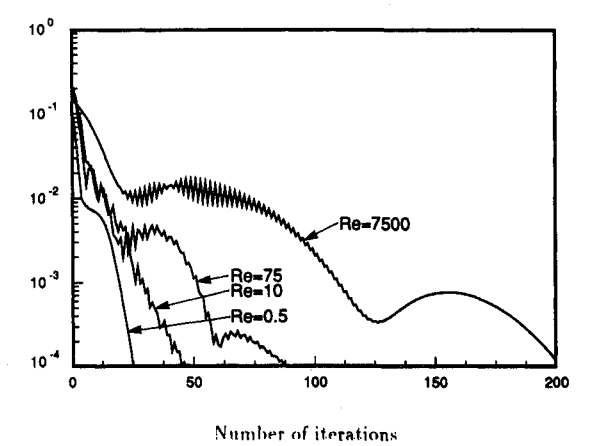

Fig. 3 Convergence history for developing flow in a two-dimensional channel inlet.

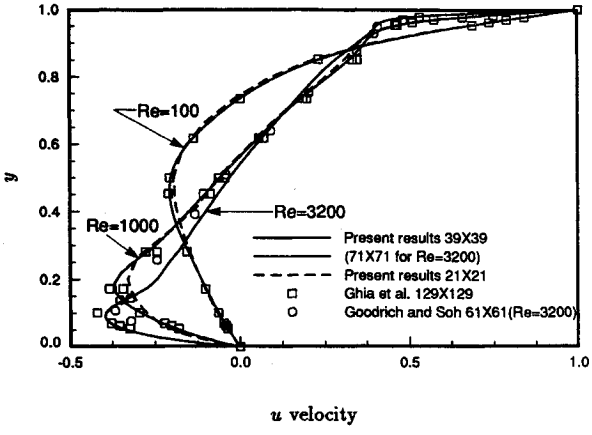

Fig. 4 Predicted u velocity component along the vertical centerline of the two-dimensional driven cavity for Re = 100, 1000, and 3200.

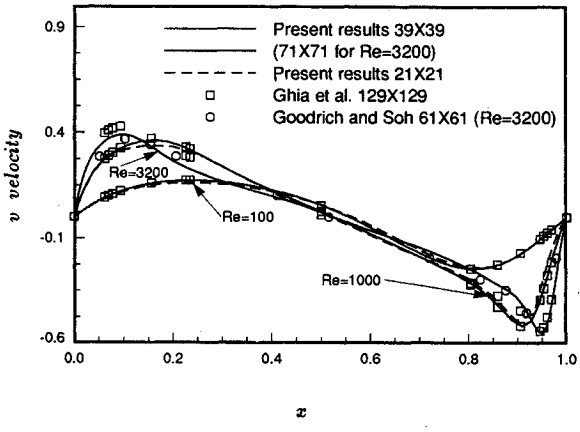

Fig. 5 Predicted v velocity component along the horizontal centerline of the two-dimensional driven cavity for Re = 100, 1000, and 3200.

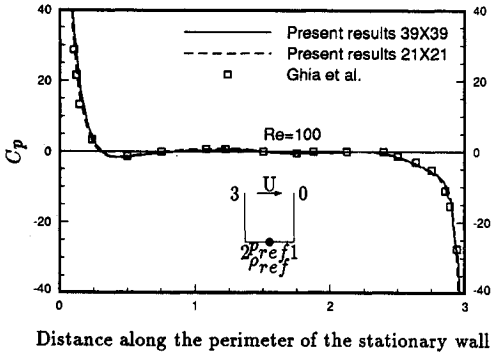

Fig. 6 Predicted pressure coefficient C_p along the stationary walls of the two-dimensional driven cavity for Re = 100 ($C_p = Re \times (\tilde{p} - \tilde{p}_{ref})/\tilde{\rho}_{ref}U^2$).

= 100 and 1000 compares very favorably with that reported by Mansour and Hamed[28] where a coupled scheme in primitive variables was used for the incompressible Navier-Stokes equations. Usually less than 200 iterations were sufficient. For the Re = 3200 case, slow convergence for a 71 × 71 grids was encountered. A similar difficulty at this Reynolds number was also reported by Napolitano and Walters.[29] It is suspected that the slow convergence at this Reynolds number is due to the strong transient nature of the flow where several significant secondary flows appear and interact with the main circulating vortex. Goodrich et al.[30] have found the flow to be unsteady at $Re \simeq 5000$.

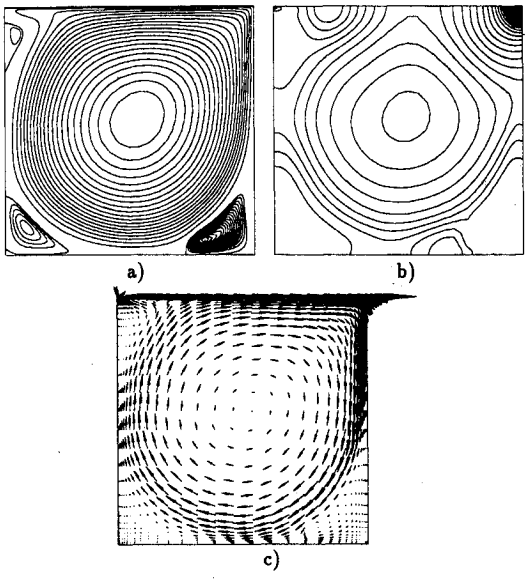

Fig. 7 Results for the two-dimensional driven cavity flow for Re = 3200: a) streamlines, b) pressure contours, and c) velocity vectors.

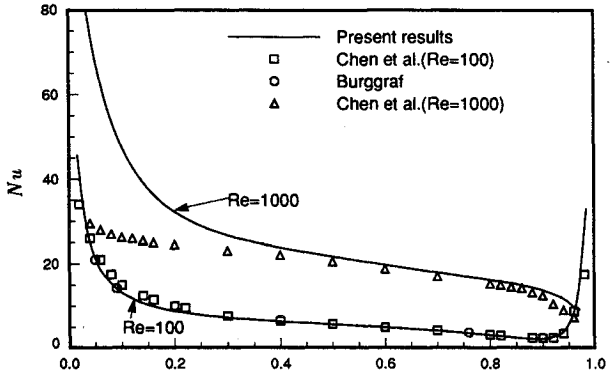

Fig. 8 Local Nusselt number at the top moving wall of the two-dimensional driven cavity.

Table 1 Mach number effect for cavity flow
Re = 100, 21 × 21 grid

Mach number	0.2	0.1	0.05	10^{-2}	10^{-3}	10^{-4}
No. of iterations	25	27	33	85	85	85

Heat-transfer results were obtained for Reynolds numbers of 100 and 1000, respectively, and a Mach number of 0.05. Figure 8 shows the local Nusselt number along the top moving wall that is hotter than the stationary wall for Re = 100 and 1000 with Pr = 1.0. The results for Re = 100 were compared with those obtained by Chen et al.[31] and Burggraf.[32] The good agreement is obvious. The results for Re = 1000, however, do not agree well with those of Chen et al.[31] near the left corner of the top wall. Further research is needed to resolve this discrepancy.

In order to study the effect of Mach number, the driven cavity case for Re = 100 with a 21 × 21 grid was computed with Mach numbers ranging from 10^{-4}–0.2 and an isothermal condition. The number of iterations (time steps) for all Mach numbers is listed in Table 1. It shows that for Mach number lower than 10^{-2} the number of iterations required increases by a factor of more than two. Even with this increase, this algorithm is still very efficient for this range of low-Mach-

number cases, at least compared with the results reported by Mansour and Hamed.[28] The solutions for the above Mach numbers were almost identical.

For all cases computed for the cavity flow, no pressure oscillation was detected using central difference even for the high Reynolds number case. This unexpected result might be attributed to 1) usage of the compressible form that contains the pressure information in the time and the first-order derivative terms and 2) the treatment of the pressure boundary condition at the wall, which employs the momentum equations to evaluate the pressure derivative at the wall in an implicit manner. Both of these procedures enhance the pressure-velocity coupling, thus tending to remove the pressure oscillation. The present authors also found the above procedures successful in removing the pressure oscillation in three-dimensional cavity flow, although the three-dimensional cavity results will not be presented here.

Unsteady Flow over a Circular Cylinder, $Re = 100$

Before solving this unsteady vortex shedding flow, the present algorithm has been tested for a flow over a circular cylinder with Reynolds number of 40 (based on diameter), which is considered[33] as the upper limit for a steady-state flow to exist for this flow configuration. The solution and efficiency of the present algorithm for this case has been discussed by Chen and Pletcher[24] and will not be included here.

This vortex shedding case was used to demonstrate the application of the present procedure for unsteady flows. This flow has been studied very extensively in the literature.[34,35] An O-type 81 × 101 grid was used with mesh clustering near the wall and in the wake region. The outer boundary was located 20 diameters from the cylinder. Since the final periodic unsteady solution was of primary interest, the initial condition was efficiently generated by the steady-state technique that quickly set up a flow pattern with a little asymmetry. The asymmetric trigger technique suggested by Lecointe and Piquet[35] was not needed. Starting from this initial solution, a constant nondimensional time step of 0.02 was used to march the solution in time. Iterations were used at each time step to eliminate the linearization error. Initially about 15 iterations were needed per time step but this number quickly dropped to two for most of the time marching history. The computation was stopped after several periodic cycles were observed. Figure 9 shows the final four cycles of the lift coefficient having a constant amplitude of about 0.31, which is almost identical to the result reported by Visbal.[36] The Strouhal number based on this is about 0.167. This result is located within the experimental range 0.16 ~ 0.17 reported by Roshko.[37]

Figure 10 shows the results for streamlines and vorticity contours, respectively, in the final cycle. The Mach number used was 0.2.

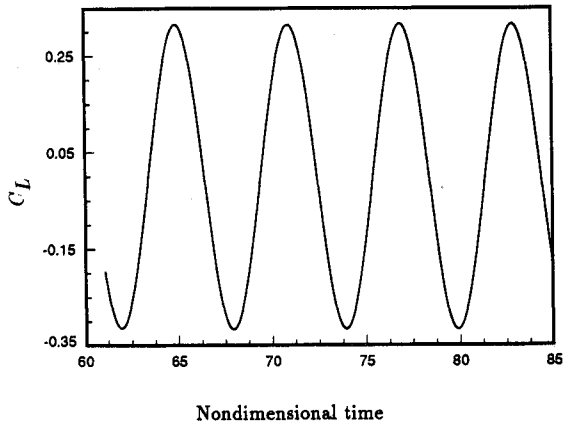

Fig. 9 Time history of the lift coefficient for the final four cycles of the vortex shedding patterns for $Re = 100$.

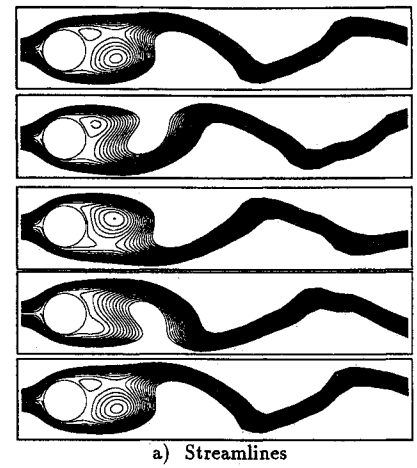
a) Streamlines

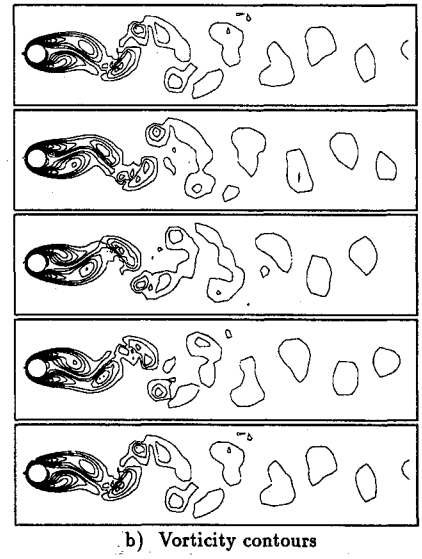
b) Vorticity contours

Fig. 10 Vortex shedding pattern for the final cycle for $Re = 100$: a) streamlines, and b) vorticity contours.

Shock-Boundary-Layer Interaction Problem

This case demonstrates the shock-capturing capability of the present procedure. This case has been studied by several other researchers,[2,3] and a more detailed description of this problem can be obtained from their work. The freestream Mach number is 2 and Reynolds number, based on the distance from the leading edge to the point at which the impinging shock intersected the plate, is 0.296×10^6. The strength of the impinging shock is strong enough to cause the laminar boundary layer to separate. The angle of this impinging shock is 32.6 deg. An 81 × 81 grid was used.

The grid was uniform in the main flow direction and stretched in the cross-stream direction with the minimum nondimensional grid increment of 1.0×10^{-4} next to the wall. The computational domain began five grid points ahead of the leading edge of the plate, and top boundary extended far enough to allow the leading-edge shock to pass through the outflow boundary. This treatment eliminates the need for using nonreflective boundary condtions at the top boundary.

Freestream conditions were specified at the inlet boundary below the impinging shock. The postshock conditions were specified at the inlet boundary above the impinging shock and along the top boundary. Extrapolation was used at the outflow boundary. Noslip conditions, zero normal pressure gradient, and an adiabatic wall temperature were used at the wall.

The results are shown for wall-pressure and skin-friction distributions in Figs. 11 and 12, respectively. The pressure contours are shown in Fig. 13. The above results compare reasonably well with the results in the literature[2,38-40] and

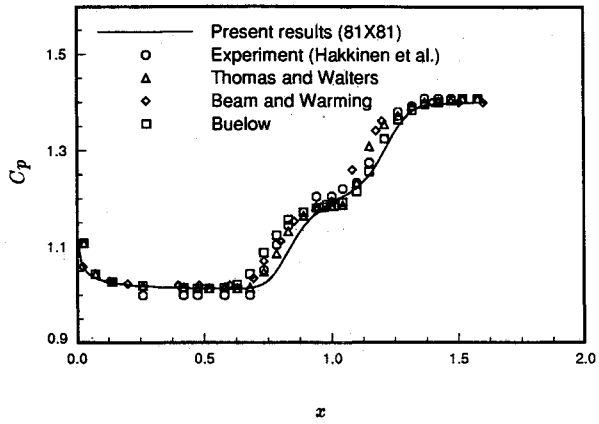

Fig. 11 Pressure-coefficient, C_p ($=\bar{p}/\bar{p}_\infty$), distribution along the wall.

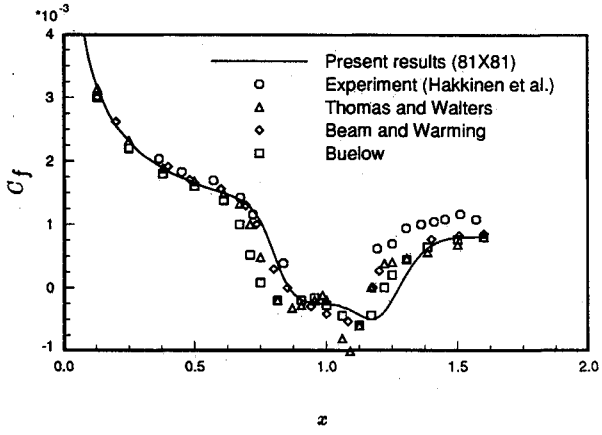

Fig. 12 Skin-friction coefficient, C_f ($=2\tau_w/Re$), distribution along the wall.

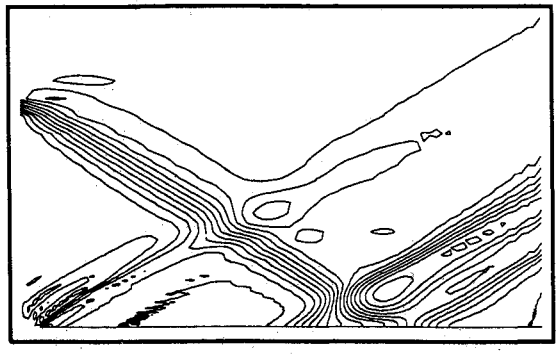

Fig. 13 Pressure contours for shock-boundary-layer interaction problem.

demonstrate the shock-capturing capability of the present scheme. About 1000 iterations were required to obtain the present converged solutions.

For this supersonic case, smoothing was needed for all variables instead of pressure only as for low-Mach-number cases. Clearly, the shock resolution obtained by this method can be improved, but the present results suggest that the formulation of the scheme is fundamentally correct and sufficient for capturing shocks.

Most of the above calculations were performed on the Apollo DN 10,000 workstation. The CPU time was approximately 0.0048 s/node/iteration.

Conclusions

A coupled solution strategy for the time-dependent compressible form of the Navier-Stokes equations that appears to be effective for Mach numbers ranging from the incompressible limit ($M_\infty \sim 0.01$) to supersonic has been developed. The approach employs the strong conservation form of the governing equations but uses primitive (u, v, p, T) variables rather than the more traditional conserved (ρ, ρu, ρv, e_t) variables as unknowns. This choice of variables simplifies the treatment of viscous terms and enhances effectiveness at low Mach numbers by allowing the density to be removed from the difference equations. A coupled modified strongly implicit procedure was used to efficiently solve the Newton-linearized algebraic equations. Generally, it was found that smoothing was not needed to control spatial oscillations in pressure for subsonic flows despite the use of central differences. Dual-time stepping was found to further accelerate convergence for steady flows. Generally good agreement between the predictions and results in the literature was observed for several test cases including steady and unsteady low-Mach-number internal and external flows and a steady shock-boundary-layer interaction flow on a flat plate in a supersonic stream. The extension of this algorithm to three-dimensional flow calculations is currently being investigated.

Acknowledgments

This research was partially supported by the Air Force Office of Scientific Research through Grant AFOSR-89-0403. The authors are also grateful for support received through a block grant from the Iowa State University Computation Center.

References

[1]Anderson, D. A., Tannehill, J. C., and Pletcher, R. H., *Computational Fluid Mechanics and Heat Transfer*, Hemisphere, New York, 1984, Chaps. 7, 9.

[2]Beam, R. M., and Warming, R. F., "An Implicit Factored Scheme for the Compressible Navier-Stokes Equations," *AIAA Journal*, Vol. 16, No. 4, 1978, pp. 393–402.

[3]Liou, M.-S., "Newton/Upwind Method and Numerical Study of Shock-Wave/Boundary-Layer Interactions," *International Journal for Numerical Methods in Fluids*, Vol. 9, No. 7, 1989, pp. 747–761.

[4]Karki, K. C., and Patankar, S. V., "Pressure-Based Calculation Procedure for Viscous Flows at All Speeds in Arbitrary Configurations," *AIAA Journal*, Vol. 27, No. 9, 1989, pp. 1167–1174.

[5]Van Doormaal, J. P., Raithby, G. D., and Mcdonald, B. H., "The Segregated Approach to Predicting Viscous Compressible Fluid Flows," *Journal of Turbomachinery, Transactions of the ASME*, Vol. 109, No. 2, April 1987, pp. 268–277.

[6]Issa, R. I., "Numerical Methods for Two- and Three-Dimensional Recirculating Flows," *Computational Methods for Turbulent, Transonic and Viscous Flows*, edited by J. A., Essecs, Hemisphere, New York, 1983.

[7]Merkle, C. L., and Choi, Y.-H., "Computation of Compressible Flows at Very Low Mach Numbers," AIAA Paper 86-0351, Jan. 1986.

[8]TenPas, P. W., and Pletcher, R. H., "Coupled Space-Marching Method for the Navier-Stokes Equations for Subsonic Flows," *AIAA Journal*, Vol. 29, No. 2, 1991, pp. 219–226.

[9]Feng, J., and Merkle, C. L., "Evaluation of Preconditioning Methods for Time-Marching Systems," AIAA Paper 90-0016, 1990.

[10]Stone, H. L., "Iterative Solution of Implicit Approximations of Multidimensional Partial Differential Equations," *SIAM Journal of Numerical Analysis*, Vol. 5, No. 3, 1968, pp. 530–558.

[11]Schneider, G. E., and Zedan, M., "A Modified Strongly Implicit Procedure for the Numerical Solution of Field Problems," *Numerical Heat Transfer*, Vol. 4, No. 1, 1981, pp. 1–19.

[12]Harlow, F. H., and Amsden, A. A., "Numerical Calculation of Almost Incompressible Flow," *Journal of Computational Physics*, Vol. 3, No. 1, 1968, pp. 80–93.

[13]Khosla, P. K., and Rubin, S. G., "Diagonally Dominant Second-Order Accurate Implicit Scheme," *Computers and Fluids*, Vol. 2, No. 2, 1974, pp. 207–209.

[14]Hindman, R. G., "Generalized Coordinate Forms of Governing Fluid Equations and Associated Geometrically Induced Errors," *AIAA Journal*, Vol. 20, No. 10, 1982, pp. 1359–1367.

[15]Chen, K.-H., *A Primitive Variable, Strongly Implicit Calculation Procedure for Two- and Three-Dimensional Unsteady Viscous Flows: Applications to Compressible and Incompressible Flows Including Flows with Free Surfaces*, Ph.D. Dissertation, Iowa State Univ., Ames, IA, 1990.

[16]Zedan, M., and Schneider, G. E., "A Coupled Strongly Implicit Procedure for Velocity and Pressure Calculation in Fluid Flow Problems," *Numerical Heat Transfer*, Vol. 8, No. 5, 1985, pp. 537–557.

[17]Walters, R. W., Dwoyer, D. L., and Hassan, H. A., "A Strongly Implicit Procedure for the Compressible Navier-Stokes Equations," *AIAA Journal*, Vol. 24, No. 1, 1986, pp. 6–12.

[18]Patankar, S. V., *Numerical Heat Transfer and Fluid Flow*, Hemisphere, New York, 1981, Chapter 6.

[19]Peyret, R., and Taylor, T. D., *Computational Methods for Fluid Flow*, Springer-Verlag, New York, 1983, pp. 104–105.

[20]Golub, G. H., and Van Loan, C. F., *Matrix Computations*, Johns Hopkins Univ. Press, Baltimore, MD, 1983, Chap. 4.

[21]Morihara, H., and Cheng, R. T., "Numerical Solution of the Viscous Flow in Entrance Region of Parallel Plates," *Journal of Computational Physics*, Vol. 11, No. 4, 1973, pp. 550–572.

[22]McDonald, J. W., Denny, V. E., and Mills, A. F., "Numerical Solutions of the Navier-Stokes Equations in Inlet Regions," *Journal of Applied Mechanics, Series E*, Vol. 39, Dec. 1972, pp. 873–878.

[23]Bodoia, J. R., and Osterle, J. F., "Finite-Difference Analysis of Plane Poiseuille and Couette Flow Development," *Applied Scientific Research, Sec. A*, Vol. 10, No. 3-4, 1961, pp. 265–276.

[24]Chen, K.-H., and Pletcher, R. H., "A Primitive Variable, Strongly Implicit Calculation Procedure for Viscous Flows at All Speeds," AIAA Paper 90-1521, June 1990.

[25]Ghia, U., Ghia, K. N., and Shin, C. T., "High-*Re* Solutions for Incompressible Flow Using the Navier-Stokes Equations and a Multigrid Method," *Journal of Computational Physics*, Vol. 48, No. 3, 1982, pp. 387–411.

[26]Goodrich, J. W., and Soh, W. Y., "Time-Dependent Viscous Incompressible Navier-Stokes Equations: The Finite-Difference Galerkin Formulation and Streamfunction Algorithm," *Journal of Computational Physics*, Vol. 84, No. 1, Sept. 1989, pp. 207–241.

[27]Ghia, K. N., Hankey, W. L., Jr., and Hodge, J. K., "Study of Incompressible Navier-Stokes Equations in Primitive Variables Using Implicit Numerical Technique," AIAA Paper 77-648, June 1977.

[28]Mansour, M. L., and Hamed, A., "Implicit Solutions of the Incompressible Navier-Stokes Equations in Primitive Variables," AIAA Paper 87-0717, August 1987.

[29]Napolitano, M., and Walters, R. W., "An Incremental Block-Line Gauss-Seidel Method for the Navier-Stokes Equations," *AIAA Journal*, Vol. 24, No. 5, 1986, pp. 770–776.

[30]Goodrich, J. W., Gustafson, K., and Halasi, K., "Hopf Bifurcation in the Driven Cavity," NASA TM-102334 (or ICOMP-89-21), Oct. 1989.

[31]Chen, C.-J., Ho, K.-S., and Cheng, W.-S., "The Finite Analytic Method," Vol. 5, IIHR Rept. 232-V, Iowa Inst. of Hydraulic Research, Univ. of Iowa, Iowa City, IA, 1982.

[32]Burggraf, O. R., "Analytic and Numerical Studies of the Structure of Steady Separated Flows," *Journal of Fluid Mechanics*, Vol. 24, Pt. 1, 1966, pp. 113–151.

[33]Fornberg, B., "A Numerical Study of Steady Viscous Flow Past a Circular Cylinder," *Journal of Fluid Mechanics*, Vol. 98, Pt. 4, 1980, pp. 819–855.

[34]Rogers, S. E., and Kwak, D., "An Upwind-Differencing Schemes for the Time-Accurate Incompressible Navier-Stokes Equations," AIAA Paper 88-2583, June 1988.

[35]Lecointe, Y., and Piquet, J., "On the Use of Several Compact Methods for the Study of Unsteady Incompressible Viscous Flow Around a Circular Cylinder," *Computers and Fluids*, Vol. 12, No. 4, 1984, pp. 255–280.

[36]Visbal, M. R., "Evaluation of an Implicit Navier-Stokes Solver for Some Unsteady Separated Flows," AIAA Paper 86-1053, May 1986.

[37]Roshko, A., "On the Development of Turbulent Wakes from Vortex Streets," NACA TN-2913, 1953.

[38]Thomas, J. L., and Walters, R. W., "Upwind Relaxation Algorithms for the Navier-Stokes Equations," AIAA Paper 85-1501, 1985.

[39]Buelow, P. E., *Comparison of TVD Schemes Applied to the Navier-Stokes Equations*, Master Thesis, Iowa State Univ., Ames, IA, 1988.

[40]Hakkinen, R. J., Greber, I., Trilling, L., and Arbarbanel, S. S., "The Interaction of an Oblique Shock Wave with a Laminar Boundary Layer," NASA Memo-2-18-59W, March 1959.